Spin Dynamics of a "Parachute" Shaped Fullerene−Porphyrin Dyad

ARTICLE *in* THE JOURNAL OF PHYSICAL CHEMISTRY A · DECEMBER 2004

Impact Factor: 2.69 · DOI: 10.1021/jp0462310

Spin Dynamics of a "Parachute" Shaped Fullerene−Porphyrin Dyad

Tamar Galili,[†] Ayelet Regev,[†] Haim Levanon,*[,†] David I. Schuster,*[,‡] and Dirk M. Guldi[§]

Department of Physical Chemistry and the Farkas Center for Light-Induced Processes, The Hebrew University of Jerusalem, Jerusalem 91904, Israel, Department of Chemistry, New York University, New York, New York 10003, and Radiation Laboratory, University of Notre Dame, Notre Dame, Indiana 46556

Received: August 20, 2004; In Final Form: September 28, 2004

The electron spin dynamics associated with the photoinduced intramolecular electron transfer (ET) in a covalently linked malonate-strapped zinc porphyrin−fullerene ($ZnP-C_{60}$) dyad with "parachute" geometry was studied by time-resolved electron paramagnetic resonance (TREPR) spectroscopy. Studies were carried out in widely different media, including solvents of different polarities, such as isotropic toluene and tetrahydrofuran, and anisotropic nematic liquid crystals, LCs (E-7 and ZLI-4389). Photoexcitation of the donor, ZnP, results in ET to the acceptor, C_{60}, in all solvents used over a wide range of temperatures. The generated radical pairs (RPs) either decay to the ground state or produce the triplet state of the acceptor moiety, $ZnP-^3*C_{60}$. Temperature-dependent studies permit the determination of the RP energy levels relative to the donor and acceptor singlet and triplet states. Thus, the results enable determination of the genesis of the ET routes as a function of the solvent polarity. Due to their unique dielectric properties, the LCs behave as solvents of low polarity at low temperatures and as solvents of high polarity at elevated temperatures. Finally, the triplet EPR line shape of $ZnP-^3*C_{60}$ oriented in the LCs verifies the asymmetric three-dimensional structure calculated recently, while the ZnP moiety in the dyad dictates the orientation of the bulky C_{60} part in the LC matrixes.

Introduction

The diversity of electron-transfer (ET) and energy-transfer (EnT) events is reflected in many fields of research such as native and model photosynthesis,[1−3] expanding into applied fields related to photovoltaic and optoelectronic devices.[4,5] It is evident that optimizing the redox properties and electronic coupling between donor and acceptor constituents, and understanding the role of their mutual orientation and the type of linkage, is of prime importance. In recent years, the study of covalently linked porphyrin−fullerene assemblies has attracted special attention.[6] In such zinc porphyrin−C_{60} systems, photoexcitation of the porphyrin (donor) leads to a chain of ET and/or EnT processes ending at the fullerene (acceptor). The small reorganization energy associated with the electron acceptor, C_{60},[7,8] accelerates the forward ET rate (charge separation) and attenuates the charge recombination (BET) rate, resulting in efficient generation of the relatively long-lived charge-separated states. Thus, not much energy is required for a charge-separated (CS) state to adjust to a different solvent environment. Moreover, the electron-accepting ability of C_{60} (~ -0.4 eV vs SCE) is similar to that of quinones,[7] while the first excited singlet and triplet states of C_{60} are much lower than those of the quinones, allowing for a strong driving force in ET and EnT reactions.

Porphyrin−fullerene systems have been synthesized by different groups, and studied extensively, mainly by ultrafast transient optical methods, providing valuable information about ET and EnT pathways in solvents of varying polarity.[9−22] On the other hand, paramagnetic transients born upon photoexcitation, such as triplets and CS states, are nonsilent entities with respect to time-resolved electron paramagnetic resonance spectroscopy (TREPR). Despite its low time resolution, TREPR provides essential and direct data on spin energetics and dynamics, thus delineating the explicit ET routes, information not available directly by transient absorption spectroscopy. Furthermore, the employment of liquid crystals (LCs), due to their extraordinary dielectric properties, broadens the scope of TREPR in these types of studies. These solvents attenuate the ET rates, thus bringing them into the TREPR time scale. Study of temperature-dependent processes is then possible over a wide range of temperatures in the mesophases.[23−28]

We report here on a TREPR study of a covalently linked zinc porphyrin−fullerene dyad **1** with a specific parachute shaped geometry (see Figure 1). This unique structure allows study of the influence of the topology of the dyad on the interaction between its donor and acceptor moieties. As will be seen, the present study provides important new information about the magnetic properties of the intermediate radical pair and triplet excited states generated upon photoexcitation of this dyad in widely different dielectric media, allowing specification of detailed pathways for their interconversion. Such information provides greater insight into the photophysics of this model donor−acceptor system than was achievable using steady state and time-resolved optical methods.

Experimental Section

The synthesis and photophysical properties of dyad **1** have been described elsewhere.[22,29,30] Using techniques described earlier,[31] continuous-wave (CW) TREPR studies of the photoexcited triplet and photoinduced charge-separated states of the

* Corresponding authors. E-mail: levanon@chem.ch.huji.ac.il (H.L.); david.schuster@nyu.edu (D.I.S.).
[†] The Hebrew University of Jerusalem.
[‡] New York University.
[§] University of Notre Dame.

10.1021/jp0462310 CCC: $27.50
Published on Web 11/09/2004

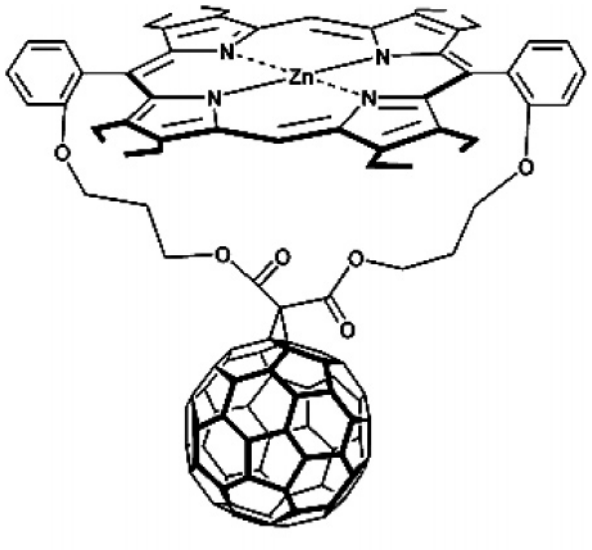

Figure 1. Structure of the "parachute" ZnP−C_{60} dyad **1**.

parachute dyad were carried out on a Bruker ESP-380 CW spectrometer with the field modulation disconnected. TREPR measurements were performed by employing different isotropic matrixes, such as toluene and tetrahydrofuran (THF) (Merck Ltd.), as well as anisotropic nematic liquid crystals (LCs) such as E-7 and ZLI-4389 (Merck Ltd.), in which the chromophores could be partially oriented. Toluene was dried over molecular sieves, and THF was distilled from sodium and benzophenone solution. The two solvents of each set were chosen due to their different dielectric constants: $\epsilon_{toluene} = 2.38$, $\epsilon_{THF} = 7.58$,[32] $\epsilon_{E-7} = 19.0$, and $\epsilon_{ZLI-4389} = 56.0$.[33] EPR samples with typical concentrations (∼0.5 mM) were prepared in 4 mm o.d. Pyrex tubes and degassed by several freeze−pump−thaw cycles on a vacuum line. Under these experimental conditions, possible aggregation is insignificant and does not affect the TREPR results. LC samples were prepared by first dissolving the chromophores in toluene, to which the LC was added after solvent evaporation.

Experiments were carried out over a broad range of temperatures, according to the phase diagrams for each solvent:

E-7: crystalline $\xrightarrow{210\ K}$ soft crystalline $\xrightarrow{263\ K}$ nematic $\xrightarrow{333\ K}$ isotropic

ZLI-4389: crystalline $\xrightarrow{250\ K}$ soft crystalline $\xrightarrow{253\ K}$ nematic $\xrightarrow{335\ K}$ isotropic

toluene: glass $\xrightarrow{117\ K}$ amorphous $\xrightarrow{178\ K}$ liquid

THF: glass $\xrightarrow{164.5\ K}$ liquid

The temperature in the EPR resonator was maintained by using a variable-temperature nitrogen flow Dewar flask.

All samples were photoexcited at 532 nm (∼10 mJ/pulse at a repetition rate of 10 Hz) by an OPO laser (Continuum Panther SLII-10) pumped by a third harmonic of a Nd:YAG laser (Continuum Surelite II-10). The photoexcitation wavelength was chosen according to the absorption spectra of the dyad's constituents, so as to mainly excite the ZnP component.

Two distinct orientations of the samples with respect to the magnetic field **B** were studied in the crystalline phase of the LCs, namely **L** || **B** and **L** ⊥ **B**, where **L** is the LC director. On

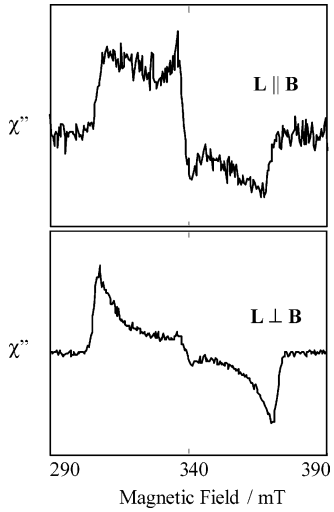

Figure 2. TREPR spectra of 1:1 mixture of ZnTPP and C_{60} oriented in E-7 at 130 K, taken at 0.9 μs after the laser pulse.

average, guest molecules will orient such that their longest axes are parallel to the direction defined by **L**.[23] The initial alignment of the sample is **L** || **B**, and the **L** ⊥ **B** orientation was obtained by rotating the sample in the microwave cavity by $\pi/2$ about an axis perpendicular to **B**. In the fluid phases, at higher temperatures (soft crystalline and nematic phases), only the **L** || **B** orientation is maintained. At these temperatures, molecular motion is allowed and rotation of the sample results in a fast molecular reorientation, back to the initial parallel configuration.

Analysis of the EPR line shape and the dynamics of the photoexcited triplets in different environments are described in detail elsewhere.[34,35] The zero field splitting (ZFS) parameters, $|\boldsymbol{D}|$ and $|\boldsymbol{E}|$, and the corresponding relative triplet population rates, A_x, A_y, and A_z, were extracted via line shape analysis. In addition, in the case of LC matrixes, the preferred orientation of the guest molecules, with respect to the director, **L**, are derived from the orientation dependence of the EPR line shape.

For comparison, control experiments were also carried out on pristine C_{60} and Zn−tetraphenylporphyrin (ZnTPP) as references for the separate dyad constituents (i.e., C_{60} and ZnP) and on a 1:1 mixture of ZnTPP and C_{60}.

Results and Discussion

Photoexcitation of a 1:1 mixture of ZnTPP and C_{60} resulted in a mixture of ^{3}*ZnTPP (dominant) and ^{3}*C_{60} TREPR spectra, in line with the extinction coefficients of the chromophores at 532 nm (Figure 2). The TREPR spectra of ^{3}*ZnTPP and ^{3}*C_{60} were previously characterized with ZFS parameters of $\boldsymbol{D} \sim 0.03$, $|\boldsymbol{E}| \sim 0.01$ and $\boldsymbol{D} \sim -0.0114$, $|\boldsymbol{E}| \sim 0.0007$ cm^{-1}, respectively.[34,36−39] In the absence of additional interactions, it is expected that selective excitation of the parachute dyad **1** should yield similar results. As will be shown below, this is not the case. First, we present the experimental observations.

Liquid Crystalline Matrixes. Figure 3 shows the TREPR spectra of dyad **1** in the crystalline phase of E-7. The spectra obtained in both LCs are similar and consist of two components, namely a narrow spectrum (∼1.5 mT) superimposed on a broad one (∼20 mT). The broad spectrum is attributed to ^{3}*C_{60}, and as will be shown below, the narrow one is attributed to the radical pair ZnP$^{\bullet+}$−$C_{60}^{\bullet-}$ (RP). No EPR spectra attributable to ^{3}*ZnP were observed over the entire temperature range. The narrow components in the center exhibit temporal phase inversion, i.e., ***a***,***e*** → ***e***,***a*** (Figure 3), where ***a*** and ***e*** indicate

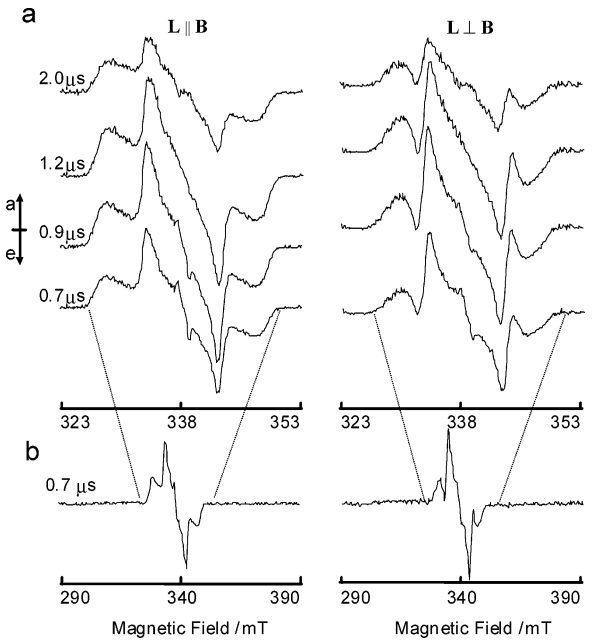

Figure 3. (a) TREPR spectra (χ'') of the dyad at 130 K oriented in E-7 at parallel and perpendicular configurations at different times after the laser pulse. (b) TREPR spectra at 0.7 μs after the laser pulse. The wider field sweep of 100 mT is to verify the absence of ^{3}*ZnTPP$-$C$_{60}$ spectra.

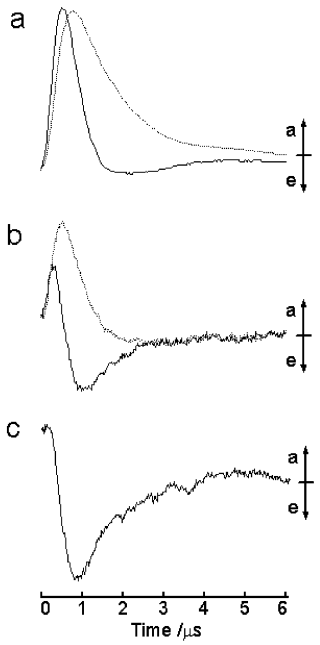

Figure 4. Kinetic traces of the dyad oriented in E-7 at the parallel configuration at 130 (a), 260 (b), and 280 K (c). The traces were recorded at 334 mT (dotted lines) and 337 mT (solid lines), corresponding to triplet (ZnP$-^3$*C$_{60}$) canonical orientation Y_2 and the RP (ZnP$^{\bullet+}-$C$_{60}^{\bullet-}$), respectively. The traces in (a) were normalized to the same intensity. Note that the dotted line is absent in (c) since the triplet (ZnP$-^3$*C$_{60}$) is not detected at this temperature.

absorption and emission patterns from low to high magnetic field, respectively. Although, the ***e***,***a*** pattern is hardly noticed at low temperatures, it is more apparent upon increasing the temperature (Figure 4). In the E-7 crystalline phase these phase patterns were observed for both sample orientations, **L** || **B** and **L** ⊥ **B**. At higher temperatures, in the nematic phases, the ^{3}*C$_{60}$ spectra and the ***a***,***e*** component of the narrow spectrum disappear. At these temperatures, only the ***e***,***a*** component of the narrow

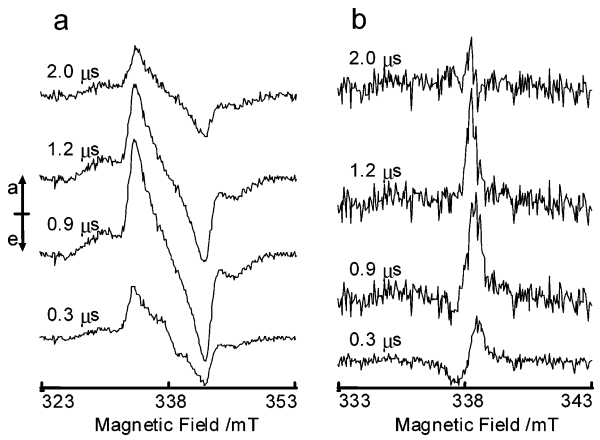

Figure 5. TREPR spectra (χ'') of the dyad at 150 K dissolved in (a) toluene and (b) THF (different scale of **B**).

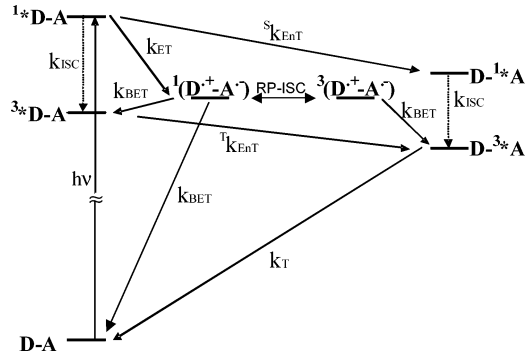

Figure 6. General presentation of the energy level scheme and the relevant processes taking place in the donor−acceptor dyad, ZnP−C$_{60}$. The energy levels of D$^{\bullet+}-$A$^{\bullet-}$ were chosen arbitrarily for the case where they lie between the ^{3}*D−A and D$-^1$*A states.

spectra is observed (Figure 4c). Above 300 K, all TREPR signals escape detection as will be discussed below.

Isotropic Matrixes. The results obtained in toluene are similar to those observed in the LCs. In particular, the spectra observed in the temperature range 130−178 K consist of the broad component attributed to ^{3}*C$_{60}$ and a narrow one characterized by an ***a***,***e*** pattern (Figure 5a). Again, no signals attributed to the ^{3}*ZnP moiety were detected. However, unlike the case of the LCs, no temporal phase inversion of the narrow component was observed in the spectra and kinetics over the entire temperature range. At temperatures above the melting point, both components disappear. The findings in THF are quite different, as only narrow signals were observed (see Figure 5b). Between 130 and 170 K the narrow spectra (∼0.8 mT) first exhibit an ***e***,***a*** pattern, which at later times (∼1 μs) evolves into a signal in absorption (Figure 5b), indicative of a spin system at thermal equilibrium.

The sequence of photoinduced processes in terms of a general donor−acceptor system is depicted in Figure 6. The discussion below is separated into two parts. The first part relates to the triplet spectra, and the second part relates to the narrow components attributed to the RP. We first exploit the triplet state as a mechanistic tool, which helps to determine the specific ET routes taking place in each solvent environment.

Triplet State. Unlike the control experiment, shown in Figure 2, dyad **1** in E-7, ZLI-4389, and toluene exhibits spectra attributable only to ^{3}*C$_{60}$ without any specific indication of ^{3}*ZnP. The absence of ^{3}*ZnP−C$_{60}$ signals is in accord with a rapid singlet-initiated ET process, ^{1}*ZnP−C$_{60}$ → RP, ZnP$^{\bullet+}-$C$_{60}^{\bullet-}$ (see below),[17,30,40] that competes with spin−orbit

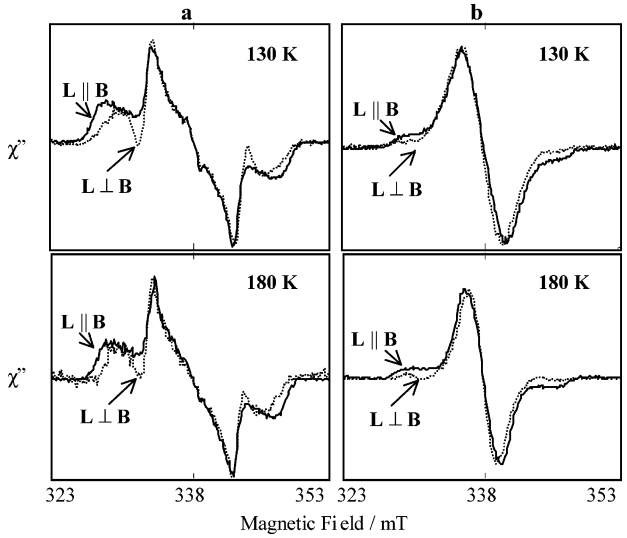

Figure 7. TREPR spectra (0.9 μs after the laser pulse) of the parachute dyad **1** (a) and pristine C_{60} (b) at 130 (upper trace) and 180 K (lower trace). The chromophores were oriented in E-7 at the parallel and perpendicular positions (indicated).

driven intersystem crossing (SO-ISC) to form ^{3}*ZnP−C_{60}. Furthermore, as was shown by earlier optical studies,[30] the RP decays by back ET (BET) either to the ground state or to the photoexcited triplet state ZnP−^{3}*C_{60}.

The TREPR spectra attributed to ^{3}*C_{60} in the dyad are characterized by ZFS parameters $|\boldsymbol{D}| = 0.01$ cm^{-1}, $|\boldsymbol{E}| = 0.0007$ cm^{-1}, typical of ^{3}*C_{60}.[41] Nevertheless, as expected for covalently linked ^{3}*C_{60}, the spectra differ from those of pristine ^{3}*C_{60} in several aspects, attributed to a significant interaction with the ZnP moiety (Figure 7). These differences are as follows:

(1) The spectra of the ZnP−^{3}*C_{60} dyad exhibit rigid-limit behavior, such that dynamic effects were not observed over the entire experimental temperature range. Rigid-limit behavior was also observed in toluene. On the other hand, pristine ^{3}*C_{60} exhibits pseudomolecular motion even at temperatures as low as 8 K, independent of the matrix.[41] In addition, whereas pristine ^{3}*C_{60} exhibits EPR signals for fast rotating triplets even in the liquid phase at room temperature and above, the spectra of the dyad were detected only in the crystalline or soft crystalline phases at much lower temperatures.

(2) The polarization pattern of pristine ^{3}*C_{60} is **a**,**a**,**a**,**e**,**e**,**e** while that of ZnP−^{3}*C_{60} is **a**,**e**,**a**,**e**,**a**,**e**, indicating different mechanisms for populating the triplet excited state, as will be discussed below.

(3) The magnetization of pristine ^{3}*C_{60} builds up slightly faster than that of ZnP−^{3}*C_{60}; e.g., at 130 K in E-7, the maximum intensity is attained after about 750 vs 900 ns, respectively.

(4) ZnP−^{3}*C_{60} exhibits unique alignment in the nematic LC matrixes which is not observed for pristine ^{3}*C_{60}. The spherical pristine ^{3}*C_{60} dissolved in a LC matrix reveals only isotropic distribution of its triplets, almost independent of the orientation of the LC's director, **L**, with respect to the external magnetic field, **B**. On the other hand, ZnP−^{3}*C_{60} does exhibit anisotropic distribution, characterized by different spectra for the parallel and perpendicular configurations of **L** with respect to **B** (see Figure 7).

We assume that the planar ZnP, to which the spherical C_{60} is covalently attached, dictates the anisotropic distribution and the rigid-limit characteristics of ZnP−^{3}*C_{60}. However, the anisotropic distribution of ZnP−^{3}*C_{60} is not typical of planar chromophores in uniaxial nematic environments such as E-7 and ZLI-4389. Specifically, all dipolar axes are observed in both the parallel and perpendicular orientations, and the outer *Z*-lines are exceptionally stronger for the parallel position. Considering the orientation dependence observed in the ZnP−^{3}*C_{60} spectra, and assuming that the ZnP moiety dictates the dyad alignment, it is concluded that the porphyrin frame of reference is tilted relative to the ZnP−^{3}*C_{60} canonical axes. In view of the fact that ^{3}*ZnP−C_{60} is not detected, the mutual orientation of the dyad constituents is manifested by the anisotropic distribution of ZnP−^{3}*C_{60} in the LC, which is enforced by the "hidden anchor", namely the ZnP moiety. This tilted relationship between the frames of reference of the ZnP and C_{60} in the dyad is in agreement with the recently calculated lowest energy molecular conformation of the dyad shown in Figure 8.[42]

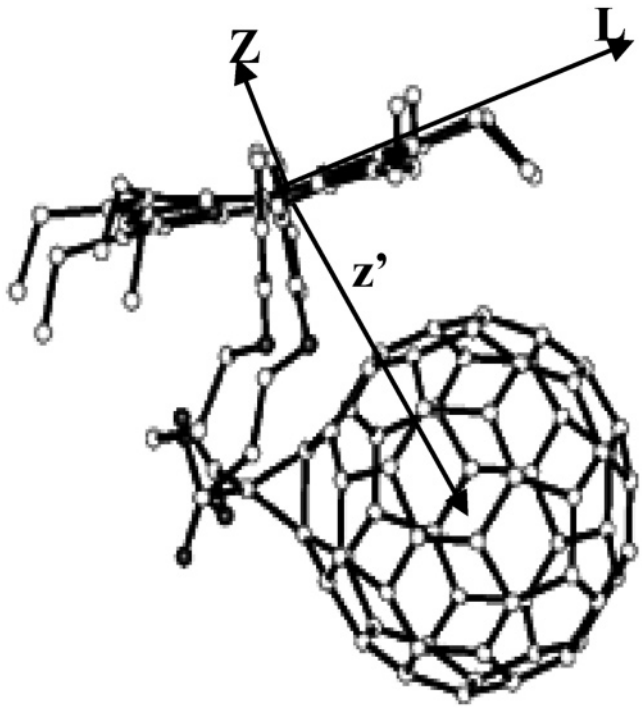

Figure 8. Calculated structure of the parachute dyad.[42] The director (**L**), the out-of-plane canonical axis (*Z*) of ^{3}*ZnP−C_{60}, and the dipolar axis of the RP, ZnP$^{\bullet+}$−$C_{60}^{\bullet-}$ (*z*′), were deduced from the TREPR analysis.

Furthermore, the observed polarization pattern **a**,**e**,**a**,**e**,**a**,**e** with $\boldsymbol{D} < 0$ and $\boldsymbol{E} > 0$ implies that the *Y* canonical orientation of ZnP−^{3}*C_{60} is selectively overpopulated, in our case via a triplet−triplet EnT mechanism. In other words, direct triplet formation via BET (singlet−triplet (ST) mixing) from ZnP$^{\bullet+}$−$C_{60}^{\bullet-}$ is not the main populating mechanism of ZnP−^{3}*C_{60}, and the indirect path via the close-lying ^{3}*ZnP−C_{60} state is much more likely. Rapid triplet−triplet EnT, namely ^{3}*ZnP−C_{60} → ZnP−^{3}*C_{60}, is also consistent with the detection only of ^{3}*C_{60} and its relatively slow generation (∼900 ns). This point will be discussed below.

Checking these conclusions by line shape analysis, employing a model of frozen pristine ^{3}*C_{60} oriented in the nematic matrix, with selective population of the *Y* canonical orientation due to EnT, proved to be unsatisfactory (simulations are not shown). This result is not surprising, given the tilted orientation of the ^{3}*C_{60} frame of reference (i.e., the triplet canonical orientations) with respect to the director, **L**. The line shape model employed takes into account the distribution of guest molecules about the director, **L**. To model the tilted orientation, the three-dimensional molecular distribution of the dyad in the nematic LC must be taken into account. Thus, at first approximation the experimental

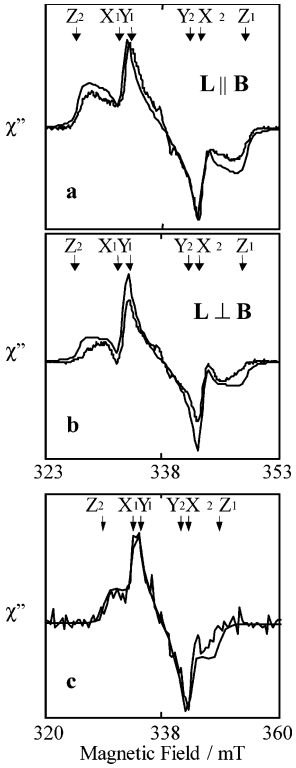

Figure 9. TREPR spectra taken at 130 K of photoexcited parachute dyad **1** in E-7 at the parallel (a) and perpendicular (b) configurations and in toluene (c). The smooth lines superimposed on the experimental spectra are line shape simulations as described in the text. The RP signals are not simulated.

spectra at each orientation of **L** ($S_{||}^{EXP}$ and $S_{\perp}^{EXP}$) were simulated with contributions of both **L** || **B** and **L** ⊥ **B** line shapes. In addition, direct BET via ST_{-1} mixing was considered as an additional route for populating ^{3}*C_{60} (see Figure 6). The smooth lines superimposed on the experimental curves in Figure 9 are computer simulations according to eqs 1 and 2:

$$S_{||}^{EXP} = 0.28S_{||}^{SIM} + 0.56S_{\perp}^{SIM} + 0.16S_{ST_{-1}}^{SIM} \quad (1)$$

$$S_{\perp}^{EXP} = 0.28S_{\perp}^{SIM} + 0.56S_{||}^{SIM} + 0.16S_{ST_{-1}}^{SIM} \quad (2)$$

where $S_{||}^{SIM}$ and $S_{\perp}^{SIM}$ are triplet line shape simulations with **L** || **B** and **L** ⊥ **B**, respectively, and $S_{ST_{-1}}^{SIM}$ is the line shape simulation for the contribution from the ST_{-1} mechanism.

The spectrum of ZnP−^{3}*C_{60} in isotropic toluene at 130 K evolves at a slow rate (~900 ns), and its characteristics are close to those obtained in the LCs. In this case, the triplet spectra could be satisfactorily fitted using the same parameters as in the LCs (Figure 9c). Upon increasing the temperature, the spectral width of ZnP−^{3}*C_{60} decreases, which could be fit by employing very slow $\pi/2$ jumps about the dipolar *Y*-axis with a rate of $\sim 1.5 \times 10^7$ s^{-1} at 170 K. This rate is 10-fold slower than that determined for pristine ^{3}*C_{60} in toluene with $\pi/2$ jumps at 8 K.[41] Similar to the behavior in the LC environment, the TREPR spectra of ZnP−^{3}*C_{60} closely follow the solvent phase transitions, and disappear above 178 K, where the isotropic liquid phase is approached.

As already mentioned, TREPR experiments using THF solutions of dyad **1** resulted only in the narrow RP signals. The absence of ZnP−^{3}*C_{60} spectra is not too surprising since the highly stabilized RP state in polar solvents is below the triplet states, and therefore is expected to decay by BET to regenerate the ground state of the dyad constituents, as previously concluded by transient absorption studies.[22,30] This point will be elaborated upon in the next section.

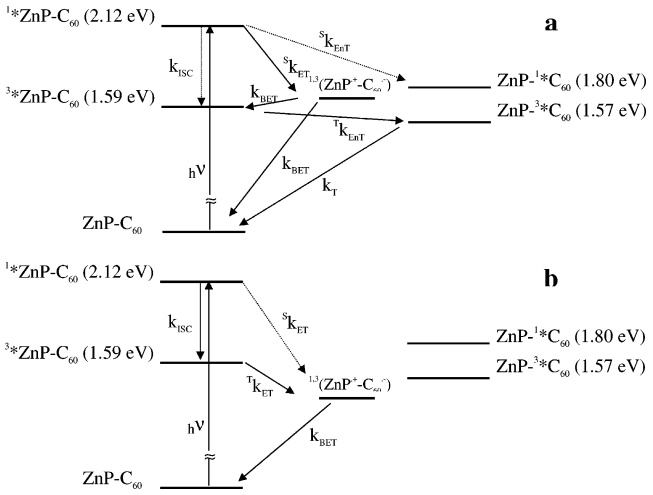

Figure 10. Energy level diagrams (unscaled) of parachute dyad **1** in (a) frozen toluene and (b) frozen THF. To reduce cluttering, the RP state ^{1,3}(Zn$^{\bullet+}$−C$_{60}^{\bullet-}$) indicates the mixing ^{1}(Zn$^{\bullet+}$−C$_{60}^{\bullet-}$) ↔ ^{3}(Zn$^{\bullet+}$−C$_{60}^{\bullet-}$).

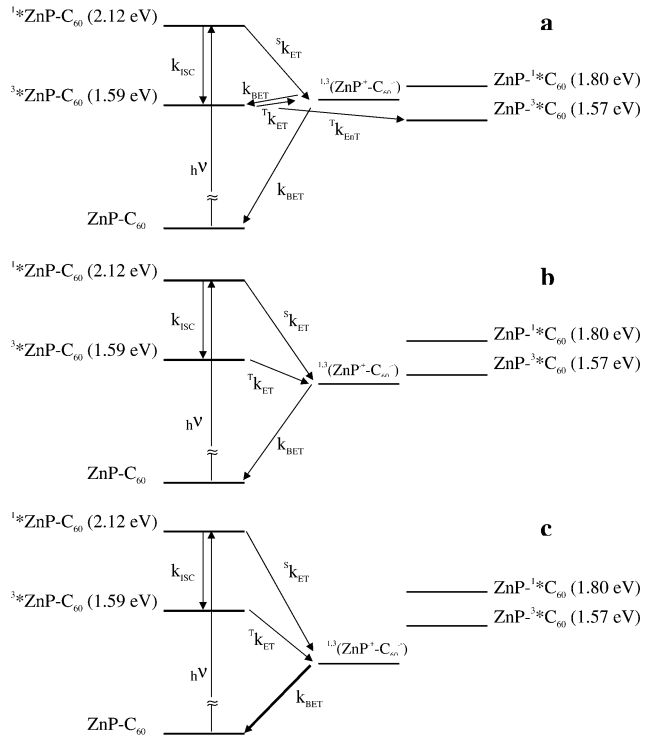

Figure 11. Energy level diagrams (unscaled) of parachute dyad **1** in (a) crystalline, (b) nematic, and (c) nematic (above 300 K) phases of E-7 and ZLI-4389. The fast BET from the low-lying RP state in (c) is indicated. To reduce cluttering, the RP state ^{1,3}(Zn$^{\bullet+}$−C$_{60}^{\bullet-}$) indicates the mixing ^{1}(Zn$^{\bullet+}$−C$_{60}^{\bullet-}$) ↔ ^{3}(Zn$^{\bullet+}$−C$_{60}^{\bullet-}$).

Radical Pair States. The narrow TREPR signals (0.8−1.5 mT), observed in all samples, and attributed to the ZnP$^{\bullet+}$−C$_{60}^{\bullet-}$ RP species, are now discussed in terms of the system energetics and dynamics in the various dielectric environments. Figures 10 and 11 describe the energetics of the RP states ZnP$^{\bullet+}$−C$_{60}^{\bullet-}$ in different environments. As mentioned above, the narrow RP signals have different polarization patterns in the two isotropic solvents used, namely ***a***,***e*** in frozen toluene and ***e***,***a*** in frozen THF. In the LCs, the RP spectra show temporal phase inversion evolving from ***a***,***e*** → ***e***,***a***. The phase inversion threshold is

temperature dependent and starts earlier upon increasing the temperature. The polarization pattern of the RP spectrum explicitly reveals its precursor, thus shedding light on the energetics of the system and the particular ET routes, i.e., via singlet vs triplet excited state precursors. Thus, the phase inversion indicates that both singlet- and triplet-initiated channels are operative. In other words, changes in the properties of the medium tune the RP energy levels with respect to the energy level of the RP precursors.

We compare the results gained with toluene to those of THF assuming that the different results are attributable only to the different dielectric constants of the solvents. This is reflected by the energy level schemes shown in Figure 10. Unfortunately, the results obtained using toluene and THF are quite limited due to the inherent properties of these isotropic solvents, which strongly affect the narrow temperature range of TREPR detection. However, the use of LCs allows extension of the temperature range within the soft glass and nematic phases. In other words, because of the nematic potential,[23] LCs can be exploited as a low polarity medium at low temperature and high polarity at high temperatures. Moreover, the nematic properties of the LCs matrixes overpower the differences in their polarity. Specifically, despite quite a large difference in polarity of E-7 and ZLI-4389, the TREPR results are similar for both LCs. Such behavior previously has been observed for other covalently linked systems.[25]

In terms of Figure 10a, the RP and triplet spectra detected by TREPR in toluene are in line with the energy and dynamics scheme concluded recently from optical data.[17,30] Specifically, in nonpolar toluene, the RP state is located above the triplet levels of both ZnP$-^{3}$*C$_{60}$ and ^{3}*ZnP$-$C$_{60}$, making ^{1}*ZnP$-$C$_{60}$ $\rightarrow$ ZnP$^{\bullet+}-$C$_{60}^{\bullet-}$ the dominant decay pathway. Placing the RP energy level below ^{1}*ZnP$-$C$_{60}$, but above ZnP$-^{1}$*C$_{60}$, would favor BET to yield ZnP$-^{1}$*C$_{60}$ followed by rapid and efficient spin$-$orbit intersystem crossing (SO-ISC) to give ZnP$-^{3}$*C$_{60}$. Under such conditions, a triplet pattern similar to that of pristine ^{3}*C$_{60}$, namely **a**,**a**,**a**,**e**,**e**,**e**, should be observed. However, the observed polarization pattern of ZnP$-^{3}$*C$_{60}$ in the parachute dyad, **a**,**e**,**a**,**e**,**a**,**e**, rules out this route. Thus, we conclude that the RP energy level in frozen toluene lies between ZnP$-^{1}$*C$_{60}$ and ^{3}*ZnP$-$C$_{60}$ (1.80 and 1.59 eV, respectively)[43] and that the RP signal with the ***a***,***e*** pattern is singlet-initiated; i.e., the RP is generated from ^{1}*ZnP$-$C$_{60}$. This assignment is consistent with optical data,[22,30] where the ET rate (k_{ET}) from ^{1}*ZnP$-$C$_{60}$ is much faster than both singlet$-$singlet EnT ($^{S}k_{EnT}$) and singlet$-$triplet SO-ISC (k_{ISC}) rates within the porphyrin moiety. The singlet-derived RP can then decay to the ground state, and/or to ^{3}*ZnP$-$C$_{60}$, and to ZnP$-^{3}$*C$_{60}$. The driving force for BET to the ground state ($>$1.59 eV) is much larger than that for the charge recombination to ^{3}*ZnP$-$C$_{60}$ (or ZnP$-^{3}$*C$_{60}$), and normally would be expected to prevail over the alternative RP decay routes. However, as shown by optical studies, this is not the case in the present system even at room temperature, indicating that the driving force for BET to ^{3}*ZnP$-$C$_{60}$ or ZnP$-^{3}$*C$_{60}$ is located in the normal region of the Marcus parabola, whereas that for BET to the ground state is in the Marcus inverted region.[44,22] Thus, BET to the ground state is much slower than the other competitive charge recombination routes.

As stated above, the observed triplet EPR signal is attributed solely to ZnP$-^{3}$*C$_{60}$. Decay of the RP via BET directly to ZnP$-^{3}$*C$_{60}$ should yield a transient spectrum typical of the RP-ISC mechanism, which could be clearly detected by TREPR, generating the "special" triplet with either the **e**,**a**,**a**,**e**,**e**,**a** pattern (for S$-$T$_0$ mixing and $\boldsymbol{D} < 0$, which is the case for ^{3}*C$_{60}$), or the **a**,**e**,**e**,**a**,**a**,**e** pattern (for S$-$T$_{-1}$ mixing).[25,45] However, this "special" triplet is not seen; thus these pathways can be ruled out. The remaining route is the RP state decay to the ^{3}*ZnP$-$ C$_{60}$ (k_{BET}) followed by triplet EnT to ZnP$-^{3}$*C$_{60}$ (k_{EnT}), which is ultimately detected by the TREPR experiments. Such a route was previously suggested by optical studies for similar fullerene$-$porphyrin dyads.[17,46,47] The optical studies on the current system were carried out only at room temperature, while our experiments were carried out at lower temperatures. The temporal behavior of the TREPR signals lends support to this route. The RP signal attains its maximum intensity within the experimental time resolution at about 200 ns, while that of ZnP$-^{3}$*C$_{60}$ reaches its maximum only after 900 ns. Such a buildup of ZnP$-^{3}$*C$_{60}$ is comparable to the decay of ZnP$^{\bullet+}-$C$_{60}^{\bullet-}$ (Figure 4), thus not allowing for a considerable buildup of the ^{3}*ZnP$-$C$_{60}$ to be observed. Above the melting point of toluene at 178 K, both signals disappear, probably due to the poor experimental time resolution relative to the relaxation processes. On the basis of the TREPR data in toluene we conclude that an indirect route to population of ZnP$-^{3}$*C$_{60}$ is operative, which allows for fine-tuning of the energy level of the RP state between those of ZnP$-^{1}$*C$_{60}$ and ^{3}*ZnP$-$C$_{60}$ (1.80 and 1.59 eV, respectively).

Similar observations are noticed in the crystalline phases of the LCs (Figure 11). With E-7, one can differentiate between the three energy levels in the crystalline, nematic, and nematic at ambient temperatures and isotropic phases. A phase inversion of the RP spectra, from ***a***,***e*** to ***e***,***a***, occurs $\sim$2 μs after laser excitation. Such behavior indicates that two routes are operative in the ET process, involving both singlet and triplet precursors, as reflected by the phase inversion pattern ***a***,***e*** $\rightarrow$ ***e***,***a***. This places the RP energy level in the crystalline phase in the vicinity of the energy level of ^{3}*ZnP$-$C$_{60}$, i.e., lower than the RP level in frozen toluene.[48] The phase inversion to ***e***,***a*** is detected, even deep in the crystalline phase (Figure 4), but is more noticeable at higher temperatures, where the RP energy level is lowered (Figure 11b). Similar to previous studies,[25,26] the triplet-initiated ET is nearly activationless, and therefore enhanced, reflecting the solvent reorganization changes in the soft crystalline and nematic phases. This change is expressed by the results in the nematic phase (above 263 K), where the RP signal exhibits only an ***e***,***a*** pattern, and no ZnP$-^{3}$*C$_{60}$ spectrum is detected. This finding indicates that at these temperatures the RP energy level drops below 1.57 eV, which is the energy level of ZnP$-^{3}$*C$_{60}$, confirming that the BET route followed by EnT is the main, if not exclusive, source of the triplet state ZnP$-^{3}$*C$_{60}$.

Such positioning of the energy level can account for the changes in the TREPR results from crystalline through soft glass to the nematic phase. The highly destabilized RP state, evident in the crystalline phase, is lowered at higher temperatures, allowing its population via the triplet pathway with an ***e***,***a*** pattern. At even higher temperatures, where the RP level further decreases, its direct population from ^{1}*ZnP$-$C$_{60}$ is too fast to be detected. The RP triplet pathway now becomes dominant, leading only to an ***e***,***a*** pattern (Figure 4c). At ambient temperatures in the nematic phase the RP escapes detection due to the fast BET to the ground state (Figure 11c).

The results in frozen THF are reminiscent of those obtained in the LCs at high temperatures, where only the RP is observed with an ***e***,***a*** pattern, due to the energetically stabilized RP level (Figure 10b). As discussed above, the absence of a ZnP$-^{3}$*C$_{60}$ spectrum can be explained by the energetics of the system. The relatively long lifetime of the RP, evident by its EPR detection

up to the phase transition of THF into liquid, points out that the driving force for BET to the ground state is in the Marcus inverted region (below 1.57 eV).[44,49,50]

In terms of Figure 6, there are two possible ET mechanisms to produce the RP states in covalently linked systems with fixed donor−acceptor distances, i.e., the triplet RP and correlated radical pair (CRP) mechanisms. The triplet RP route was observed previously in covalently linked systems with short donor−acceptor distances of ∼11 Å or less, where single-step ET occurs.[26,27,51] CRP spectra have been observed in many covalently linked molecular systems where the donor−acceptor distances, r_{c-c}, are ∼20 Å, in which case a two-step ET mechanism takes place.[25,26,28] In the parachute system in which the donor−acceptor distance, r_{c-c}, is 7.8 Å,[22,42] the observed RPs are expected to be triplet, i.e., $^3(ZnP^{\bullet+}-C_{60}^{\bullet-})$. For the singlet-initiated ET process, where the triplet RP spectrum is generated via RP-ISC through ST_0 mixing (Figure 6), the selected population is via the T_0 level. For $\boldsymbol{D} < 0$, which is common for ET processes, one would expect a triplet pattern of **e**,**a**,**a**,**e**,**e**,**a**. For $\boldsymbol{E} = 0$ (axial configuration), usually found in RPs, the polarization pattern is **e**,**a**,**e**,**a**. Thus, the ***a***,***e*** narrow signal in the center of the spectra is proposed to be due to the central lines of the triplet RP spectrum. In this case, the narrow signals are characterized by the same ***a***,***e*** pattern, for both $\mathbf{L} \parallel \mathbf{B}$ and $\mathbf{L} \perp \mathbf{B}$ configurations, according to the triplet RP mechanism. In the case of CRP spectra, a change in the polarization pattern often occurs with sample rotation.[25,26] For $r_{c-c} = 7.8$ Å, the ZFS $\boldsymbol{D}$ values may be estimated through the dipole−dipole approximation ($|\boldsymbol{D}| \approx (3/4)(g\beta)^2/r_{c-c}^3$) to be ∼5.7 mT. Thus, the triplet RP spectral width should be of the same order of magnitude as that of $ZnP-{}^3{*}C_{60}$ when the intense $ZnP-{}^3{*}C_{60}$ spectrum veils the weak triplet RP spectrum.

In the case of triplet-initiated ET in frozen THF and in LCs at high temperatures, the triplet RP spectrum develops by polarization transfer from $^3{*}ZnP-C_{60}$ to $^3(ZnTPP^{\bullet+}-C_{60}^{\bullet-})$.[52−55] Inspection of the molecular structure of the parachute system (Figure 8) suggests that the *Z*-axis of $^3{*}ZnP-C_{60}$ is almost parallel to the z' dipolar axis of $^3(ZnP^{\bullet+}-C_{60}^{\bullet-})$. Thus, it is reasonable to assume that the triplet RP sublevel associated with the z'-axis is mainly populated via $^3{*}ZnP-C_{60}$. In such a case, with $\boldsymbol{D} < 0$, an overall **e**,**e**,**e**,**a**,**a**,**a** pattern is expected for the $^3(ZnP^{\bullet+}-C_{60}^{\bullet-})$ spectrum. Moreover, as in the case of triplet RP initiated from a singlet precursor, the observed ***e***,***a*** polarization pattern may arise from the degenerate central lines ($\boldsymbol{E} = 0$), since the outmost z' lines escape detection due to molecular motion, and the anisotropic line broadening resulting in a poor signal-to-noise ratio (Figure 5b). This unfortunately prevents determination experimentally of the center-to-center distance in $ZnP-C_{60}$. Nevertheless, the observed RP spectra showing different polarization patterns, together with the threshold of appearance or disappearance of the triplet spectra of the acceptor C_{60} in the dyad, allow specification of the precise ET and BET routes operating in these systems.

Conclusions

The results of this TREPR study of the porphyrin−fullerene dyad **1** shown in Figure 1 are in excellent agreement with those derived from photophysical studies[22] and provide considerable additional information. It was demonstrated previously that extremely rapid photoinduced ET occurs at ambient temperatures in both polar and nonpolar solvents to give a charge-separated RP state, whose energy level lies above that of $ZnP-{}^3{*}C_{60}$ in nonpolar solvents and below it in polar solvents. The results of the present TREPR study are entirely in accord with this conclusion, as shown in Figure 10. The precise route for formation of $ZnP-{}^3{*}C_{60}$ from the RP state could not be deduced from the optical experiments, but it is clear from TREPR data. Thus, we can conclude that that BET occurs first to give $^3{*}ZnP-C_{60}$, which then undergoes triplet−triplet EnT to give $ZnP-{}^3{*}C_{60}$, representing a new mechanistic insight into the overall photodynamics of this model donor−acceptor system. Furthermore, the polarization pattern of the RP spectrum explicitly reveals the spin multiplicity of the RP precursors, and provides information about the energetics of the various intermediates in the system, as depicted in Figure 10, and the precise pathway followed after photoexcitation.

The mutual orientation of the dyad constituents is evident by the anisotropic distribution of $ZnP-{}^3{*}C_{60}$ in the LC. This tilted relationship between the frames of reference of the ZnP and C_{60} in the dyad is in agreement with the recently calculated molecular conformation of the dyad.[42] To our knowledge, the photophysics of porphyrin−fullerene dyads and related arrays has not been previously studied in LC media. The ability to alter the local dielectric constant by changing the LC phase as a function of temperature presents a new technique in this area of research for changing the overall photophysical behavior, by raising or lowering the energy of the RP state relative to the energies of the electronic excited states of the system.

This study clearly demonstrates the advantage of LCs over traditional isotropic solvents in determining the ET and/or EnT routes following photoexcitation of a typical donor−acceptor system. The ability to generate charge-separated states with different energies, as a function of temperature, is unique to LCs because of their special dielectric properties. For example, by changing the temperature of the LC environment, it is possible to tune the RP energy levels to fit with a variety of solvents of different polarities. This is manifested by the resemblance of the low-temperature behavior of the LC system to toluene, while increasing the temperature causes the LC system to behave as a typical polar solvent, in our case THF.

Acknowledgment. The Farkas Center is supported by the Bundesministerium Forschung und Technologie and the Minerva Gesellschaft für die Forschung GmbH. This work was partially supported by the Israel Science Foundation (H.L.), the U.S.−Israel Binational Science Foundation (H.L.), and the Ministry of Science (H.L.). The work at NYU was supported by grants from the US National Science Foundation. Research at Notre Dame is supported by the US Department of Energy. This is Contribution No. NDRL-4546 from the Radiation Laboratory. Discussions with Dr. A. Berg and Mr. E. Stavitski are highly appreciated.

References and Notes

(1) Fox, M. A. *Photoinduced Electron Transfer*; Elsevier: Amsterdam, 1988.

(2) Wasielewski, M. R. *Chem. Rev.* **1992**, *92*, 435.

(3) Levanon, H.; Möbius, K. *Annu. Rev. Biophys. Biomol. Struct.* **1997**, *26*, 495.

(4) Cravino, A.; Sariciftci, N. S. *J. Mater. Chem.* **2002**, *12*, 1931.

(5) Yamada, H.; Imahory, H.; Nishimura, Y.; Yamazaki, I.; Ahn, T. K.; Kim, S. K.; Kim, D.; Fukuzumi, S. *J. Am. Chem. Soc.* **2003**, *125*, 9129.

(6) Bracher, P. J.; Schuster, D. I. Electron Transfer in Functionalized Fullerenes. In *Fullerenes: From Synthesis to Optoelectronic Applications*; Guldi, D. M., Martin, N., Eds.; Kluwer Academic Publishers: Dordrecht, 2002; p 163.

(7) Imahori, H.; Hagiwara, K.; Akiyama, T.; Aoki, M.; Taniguchi, S.; Okada, T.; Shirakawa, M.; Sakata, Y. *Chem. Phys. Lett.* **1996**, *263*, 545.

(8) Guldi, D. M. *Chem. Commun.* **2000**, 321.

(9) Martin, N.; Sanchez, L.; Illescas, B.; Perez, I. *Chem. Rev.* **1998**, *98*, 2527.

(10) Bourgeois, J. P.; Diederich, F.; Echegoyen, L.; Nierengarten, J. F. *Helv. Chim. Acta* **1998**, *81*, 1835.
(11) Dietel, E.; Hirsch, A.; Eichhorn, E.; Rieker, A.; Hackbarth, S.; Roder, B. *Chem. Commun.* **1998**, 1981.
(12) Fong, R.; Schuster, D. I.; Wilson, S. R. *Org. Lett.* **1999**, *1*, 729.
(13) MacMahon, S.; Fong, R.; Baran, P. S.; Safonov, I.; Wilson, S. R.; Schuster, D. I. *J. Org. Chem.* **2001**, *66*, 5449.
(14) Schuster, D. I. *Carbon* **2000**, *38*, 1607.
(15) Gust, D.; Moore, T. A.; Moore, A. L. *J. Photochem. Photobiol., B* **2000**, *58*, 63.
(16) Guldi, D. M. *Chem. Soc. Rev.* **2002**, *31*, 22.
(17) Guldi, D. M.; Martin, N. *J. Mater. Chem.* **2002**, *12*, 1978.
(18) Moore, T. A.; Moore, A. L.; Gust, D. *Philos. Trans. R. Soc. London, Ser. B* **2002**, *357*, 1481.
(19) Imahori, H.; Mori, Y.; Matano, Y. *J. Photochem. Photobiol., C* **2003**, *4*, 51.
(20) Tkachenko, N. V.; Lemmetyinen, H.; Sonoda, J.; Ohkubo, K.; Sato, T.; Imahori, H.; Fukuzumi, S. *J. Phys. Chem. A* **2003**, *107*, 8834.
(21) Kesti, T.; Tkachenko, N.; Yamada, H.; Imahori, H.; Fukuzumi, S.; Lemmetyinen, H. *Photochem. Photobiol. Sci.* **2003**, *2*, 251.
(22) Schuster, D. I.; Cheng, P.; Jarowski, P. D.; Guldi, D. M.; Luo, C.; Echegoyen, L.; Pyo, S.; Holzwarth, A. R.; Braslavsky, S. E.; Williams, R. M.; Klihm, G. *J. Am. Chem. Soc.* **2004**, *126*, 7257.
(23) Levanon, H.; Hasharoni, K. *Prog. React. Kinet.* **1995**, *20*, 309.
(24) Levanon, H. *Adv. Photosynth.* **1996**, *3*, 211.
(25) Hasharoni, K.; Levanon, H.; Greenfield, S. R.; Gosztola, D. J.; Svec, W. A.; Wasielewski, M. R. *J. Am. Chem. Soc.* **1996**, *118*, 10228.
(26) Levanon, H.; Galili, T.; Regev, A.; Wiederrecht, G. P.; Svec, W.; Wasielewski, M. R. *J. Am. Chem. Soc.* **1998**, *120*, 6366.
(27) Wiederrecht, G. P.; Svec, W. A.; Wasielewski, M. R.; Galili, T.; Levanon, H. *J. Am. Chem. Soc.* **2000**, *122*, 9715.
(28) Shaakov, S.; Galili, T.; Stavitski, E.; Levanon, H.; Lukas, A.; Wasielewski, M. R. *J. Am. Chem. Soc.* **2003**, *125*, 6563.
(29) Cheng, P.; Wilson, S. R.; Schuster, D. I. *Chem. Commun.* **1999**, 89.
(30) Schuster, D. I.; Cheng, P.; Wilson, S. R.; Prokhorenko, V.; Katterle, M.; Holzwarth, A. R.; Braslavsky, S. E.; Klihm, G.; Williams, R. M.; Luo, C. P. *J. Am. Chem. Soc.* **1999**, *121*, 11599.
(31) Berg, A.; Galili, T.; Levanon, H.; Kotlyar, A. B.; Hazani, M. *J. Phys. Chem.* **1999**, *103*, 8372.
(32) Honeywell, B. J. http://www.bandj.com/BJSolvents; 2004.
(33) Merck, E. *Merck Ltd. Catalog: Nematic Liquid Crystal Mixtures*, 1989.
(34) Gonen, O.; Levanon, H. *J. Chem. Phys.* **1986**, *84*, 4132.
(35) Regev, A.; Galili, T.; Levanon, H. *J. Phys. Chem.* **1996**, *100*, 18502.
(36) Gonen, O.; Levanon, H. *J. Phys. Chem.* **1985**, *89*, 1637.
(37) Wasielewski, M. R.; O'Neil, M. P.; Lykke, K. R.; Pellin, M. J.; Gruen, D. M. *J. Am. Chem. Soc.* **1991**, *113*, 2774.
(38) Levanon, H.; Michaeli, S.; Meiklyar, V. *Triplet dynamics of C60 and C70 and its participation in electron transfer reactions. Time-resolved electron paramagnetic resonance*; The Electrochemical Society: Pennington, NJ, 1994; Vol. 1.
(39) Groenen, E. J. J.; Poluektov, O. G.; Matsushita, M.; Schmidt, J.; van der Waals, J. H. *Chem. Phys. Lett.* **1992**, *197*, 314.
(40) Kuciauskas, D.; Lin, S.; Seely, G. R.; Moore, A. L.; Moore, T. A.; Gust, D.; Drovetskaya, T.; Reed, C. A.; Boyd, P. D. W. *J. Phys. Chem.* **1996**, *100*, 15926.
(41) Regev, A.; Gamliel, D.; Meiklyar, V.; Michaeli, S.; Levanon, H. *J. Phys. Chem.* **1993**, *97*, 3671.
(42) Schuster, D. I.; Jarowski, P. D.; Kirschner, A. N.; Wilson, S. R. *J. Mater. Chem.* **2002**, *12*, 2041.
(43) Fujisawa, J.; Ohba, Y.; Yamauchi, S. *Chem. Phys. Lett.* **1998**, *294*, 248.
(44) Marcus, R. A. *J. Chem. Phys.* **1956**, *24*, 966.
(45) Norris, J. R.; Morris, A. L.; Thurnauer, M. C.; Tang, J. *J. Chem. Phys.* **1990**, *92*, 4239.
(46) Guldi, D. M.; Luo, C. P.; Prato, M.; Dietel, E.; Hirsch, A. *Chem. Commun.* **2000**, 373.
(47) Guldi, D. M.; Scheloske, M.; Dietel, E.; Hirsch, A.; Troisi, A.; Zerbetto, F.; Prato, M. *Chem. Eur. J.* **2003**, *9*, 4968.
(48) The ideal theoretical model where all RP energy levels are not affected by the solvent reorganization is true for frozen matrixes. In our case it seems that this rule is somewhat violated at the experimental temperature (130 K). This may suggest that at this temperature the solvent matrixes, accommodating the RP system, have some degree of freedom.
(49) Miller, J. R.; Calcaterra, L. T.; Closs, G. L. *J. Am. Chem. Soc.* **1984**, *106*, 3047.
(50) Closs, G. L.; Calcaterra, L. T.; Green, N. J.; Penfield, K. W.; Miller, J. R. *J. Phys. Chem.* **1986**, *90*, 3673.
(51) Wiederrecht, G. P.; Svec, W. A.; Wasielewski, M. R.; Galili, T.; Levanon, H. *J. Am. Chem. Soc.* **1999**, *121*, 7726.
(52) Hasharoni, K.; Levanon, H.; von Gersdorff, J.; Kurreck, H.; Möbius, K. *J. Chem. Phys.* **1993**, *98*, 2916.
(53) Hasharoni, K.; Levanon, H.; Gätschmann, J.; Schubert, H.; Kurreck, H.; Möbius, K. *J. Phys. Chem.* **1995**, *99*, 7514.
(54) Kurreck, H.; Huber, M. *Angew. Chem., Int. Ed. Engl.* **1995**, *34*, 849.
(55) Da Ros, T.; Prato, M.; Guldi, D. M.; Ruzzi, M.; Pasimeni, L. *Chem. Eur. J.* **2001**, *7*, 816.